

# Tracking of Fluctuating Load Power Quality Using Normalized Embedded Zero-tree Wavelet Coding Considering Data Compression

SHU-CHEN WANG

Department of Computer and Communication Engineering  
Taipei College of Maritime Technology  
Taipei, Taiwan  
scwang@mail.tcmt.edu.tw

CHENG-PING HUANG

Department of Mechatronic Engineering, Dahan Institute of Technology,  
Hualien, Taiwan

CHI-JUI WU,

Dep. of Electrical Engineering, National Taiwan University of Science and Technology  
Taipei, Taiwan  
cjwu@mail.ntust.edu.tw

*Abstract:* - In this paper, the data compression technique using the normalized embedded zero-tree wavelet (NEZW) coding is presented for the long-duration monitoring of a DC electric arc furnace and a railroad tracking load. For those power quality disturbing loads, harmonics, voltage fluctuation, and loading fluctuation are critical and stochastic load characteristics. In the power quality measurement, while keep enough stochastic load information, it is desired to reduce data size in long duration recording of voltage and current waveforms. The effects of multi-resolution analysis levels and threshold values in the NEZW coding are investigated. From the calculation results of field measurement data, the NEZW coding almost preserves the values of voltage fluctuation and power quantities. For storage of the field measurement voltage and current waveforms, the NEZW coding can not only greatly reduce data size, but it also can preserve sufficient load information.

*Key-Words:* - electric power quality, data compression, discrete wavelet transform, multi-resolution analysis, normalized embedded zero-tree wavelet coding.

## 1 Introduction

Stochastic fluctuating loads, such as electric arc furnaces (EAFs), may cause the disturbances of voltage fluctuation (voltage fluctuation) [1-8]. The voltage and current waveforms of EAFs may be different cycle from cycle due to the stochastic behaviors. Thereby the values of active and reactive power will change cycle by cycle. However, it is sometimes desired to record the voltage and current waveforms for a long duration to track the disturbance levels. The instantaneous waveforms are helpful in determining mitigation methods and devices. But the recording of instantaneous three-phase voltage and current waveforms, a few seconds period (hundreds of power cycles) would need memory high to several mega bytes. Therefore, in consideration of memory space and cost down, the recorded data length of an instrument will be limited. How to effectively reduce the data size becomes a very important issue.

There are basically many approaches in data compression. While lossless data compression wants to keep full signal information, lossy data compression gives better compression ability considering acceptable errors. The later generally uses a suitable transform to analyze the data and therefore a coding method is to extract the characteristic information and remove redundancy. Many transform methods have been used, such as discrete Fourier transform, short-term discrete Fourier transform, discrete cosine transform (DCT), and discrete wavelet transform (DWT) [9-15]. The DWT is a good transform for preserving feature integrity and removing redundancy to obtain a higher compression result. It is effective in localizing analysis of time-sequence sampled data by the time-frequency domain characteristics. There are several representatives of state-of-art coders, such as embedded zero-tree wavelet coding (EZW) [16], embedded zero-tree DCT coding, zero-tree entropy coding, set partition in hierarchical trees coding,

embedded block coding with optimized truncation [17], and vector quantization (VQ) coding [18, 19]. For example, the EZW coding is the data compression algorithm of JPEG2000 [14, 15]. It has been applied to the compression of medical electrocardiogram data [20].

In this paper, the DWT with the normalized embedded zero-tree wavelet (NEZW) coding, is presented and used as a data compression method for long-duration recoding purposes. The approach is to enhance the storage capacity in recording instantaneous three-phase voltage and current waveforms of disturbing loads, where voltage fluctuation and loading fluctuation are major disturbances. A DC EAF and a railway electrification substation are examined. The compression results are compared with the well-known threshold (TH) coding and vector quantization (VQ) coding. The differences of voltage fluctuation values between original waveforms and reconstructed waveforms could be used to demonstrate that this approach can track voltage fluctuation well. The errors in integral values of arithmetic apparent power, fundamental active power, and fundamental reactive power are also used to reveal that the data compression approach can keep the information of load fluctuating.

## 2 Wavelet Transform

The continuous wavelet transform of signal  $x(t)$  is

$$CWT(a,b) = \langle x(t), \psi_{a,b}(t) \rangle = \int_{-\infty}^{+\infty} x(t) \psi_{a,b}(t) dt \quad (1)$$

$$\psi_{a,b}(t) = \psi((t-b)/a) / \sqrt{a} \quad (2)$$

where  $a$  is the scale parameter, and  $b$  is the time shift parameter. The wavelet basic function  $\psi_{a,b}(t)$  is defined on the right half plane of  $(a, b)$ , that is,  $(b \in \mathbf{R}, a > 0)$ . The original signal  $x(t)$  can be reconstructed by the parameter  $(a, b)$ . The inverse continuous wavelet transform is given by

$$x(t) = \frac{1}{C_\psi} \int_{-\infty}^{+\infty} \int_{-\infty}^{+\infty} CWT(a,b) \psi_{a,b}(t) \frac{dadb}{a^2} \quad (3)$$

where  $C_\psi$  is the normalized constant.

For a digital recorder with a sampling period  $T$ , the discrete wavelet transform (DWT) is needed. Selecting  $a=a_0^m$ ,  $b=na_0^m b_0$ ,  $t=kT$ , and  $k, m, n \in \mathbf{Z}$ , the DWT is

$$DWT(m,n) = \langle x[k], \psi_{m,n}[k] \rangle = \sum_k x[k] \psi^*[(k-na_0^m b_0)/a_0^m] \quad (4)$$

The inverse discrete wavelet transform (IDWT) is given by

$$x[k] = \left( \sum_m \sum_n DWT(m,n) \psi^*[(k-na_0^m b_0)/a_0^m] \right) / C_\psi \quad (5)$$

Equation (4) could be said to an FIR filter with  $\psi(k)$  as the impulse response of the digital filter. So we can use multi-resolution filters to achieve DWT or IDWT.

## 3 Normalized Embedded Zero-Tree Wavelet (NEZW) Coding

If the DWT is applied to data compressing, it will relate to the address characteristics of wavelet set in multi-resolution analysis (MRA). The original signal is decomposed to several levels. The NEZW coding is used to extract the characteristic information and remove the redundancy as shown in Fig. 1, where a 3-level MRA decomposition and reconstruction method is given. In the  $s^{\text{th}}$ -level,  $s=1, 2, \text{ and } 3$ ,  $C_{s-1}[n]$  is resolved into  $C_s[n]$  and  $D_s[n]$ , where the high frequency band coefficients  $D_s[n]$  will be processed through the NEZW coding. The coefficients in wavelet decomposition form an inverted hierarchical pyramid, with the coarsest scale components at the bottom and the finest scale components at the top. In the interior of the pyramid, each coefficient of  $D_s[n]$  has two children at the next finer scale,  $D_{s-1}[2n]$  and  $D_{s-1}[2n+1]$ , which correspond to the same spatial locations as  $D_s[n]$ . If the original signal  $C_0[n]$  is normalized, it can let magnitudes of all  $D_s[n]$  be less than 2 in each level. Therefore, in contrast to EZW, the NEZW algorithm can adopt 1 (i.e.  $2^0$ ) to be the initial threshold value instead of searching the initial threshold value through all  $D_s[n]$  for any original signal  $C_0[n]$ . Figure 2 shows an example of the high frequency band coefficients for a sampled signal in a 3-level MRA. The significance of a coefficient is determined by comparing its magnitude with a set of gradually decreasing thresholds. The forward wavelet transform concentrates its information into a relatively small number of coefficients with large magnitude. That is, the NEZW prioritization scheme transmits the large (significant) coefficients before transmitting the smaller (insignificant) coefficients. The choices of thresholds in this paper would be  $2^0, 2^{-1}, 2^{-2}, 2^{-3}, 2^{-4}$ , and so on. The effect is like as factorization in mathematics. Suppose the minimum threshold value of NEZW coding is limited to  $2^{-4}$ , the coding algorithms are as follows. Figure 3 demonstrates the synopsis for the example in Fig. 2.

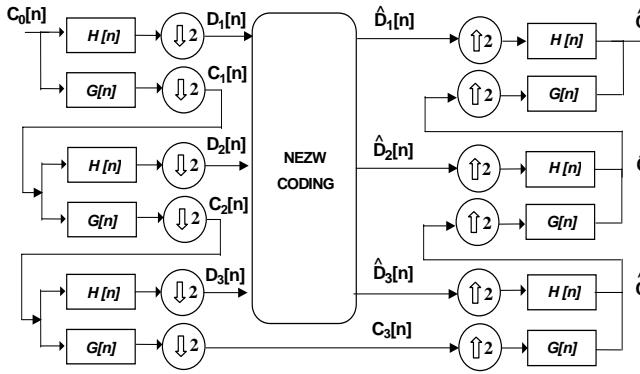


Fig. 1. Decomposition and reconstruction using 3-level multi-resolution analysis and NEZW coding.

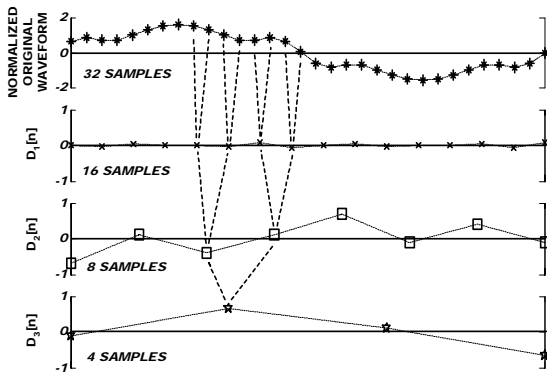


Fig. 2. The inverted hierarchical pyramid parent-child relationships for one tree of wavelet coefficients.

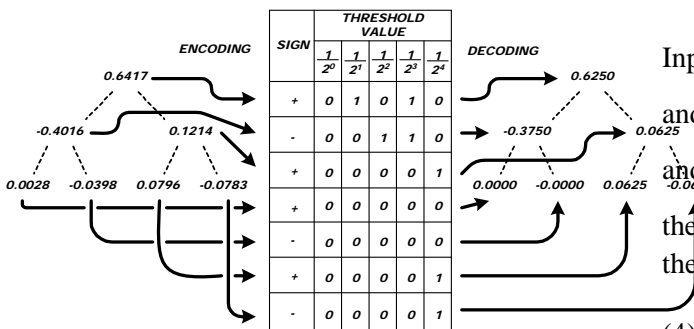


Fig. 3. The schema of NEZW coding for the example of Fig. 2.

### 3.1 Encoding Algorithm

The original signal is split into non-overlapping blocks of samples. Each block is transformed and encoded separately. The blocking approach allows compression to be done in real time. Let RL (the refinement list) be the list of coefficients which have previously been found to be significant, and let SL (the search list) be the list of coefficients which have not yet been found to be significant. The compression algorithm is as follows.

- (1) Set  $k=0$  and set RL to empty.

- (2) For each  $D_s[n]$  in RL, output the most significant bit of  $D_s[n]$ .
- (3) Set SL to be all the coefficients except those in RL, ordered so that parents are listed before their children. For each  $D_s[n]$  in SL:  
If  $D_s[n] \geq 2^{-k}$ , then output POS to the symbol S and add  $D_s[n]$  to RL; else if  $D_s[n] \leq -2^{-k}$  then output NEG and add  $D_s[n]$  to RL, else if no descendant of  $D_s[n]$  is significant, i.e.,  $2^{-k} > D_s[n] > -2^{-k}$ , then output ROOT and remove all the descendants of  $D_s[n]$  from SL, else output ZERO.
- (4) If  $k \leq 4$ , then increase  $k$  by one and go to Step (2).

### 3.2 Decoding Algorithm

The decoding algorithm is as follows:

- (1) Let  $k=0$ , set RL to empty, and set all  $\hat{D}_s[n]$  to zero.
- (2) For each  $\hat{D}_s[n]$  in RL, input the most significant bit of  $\hat{D}_s[n]$ .
- (3) Set SL to be all the coefficients except those in RL, ordered so that parents are listed before their children. For each  $\hat{D}_s[n]$  in SL:  
Input a symbol S. If S=POS then set  $\hat{D}_s[n]$  to  $2^{-k}$  and add to RL; else if S=NEG then set  $\hat{D}_s[n]$  to  $-2^{-k}$  and add  $\hat{D}_s[n]$  to RL; else if S=ROOT then remove all the descendants of  $\hat{D}_s[n]$  from SL; else if S=ZERO then do nothing.
- (4) If  $k \leq 4$ , then increase  $k$  by one and go to Step (2).

## 4 Characteristics of Fluctuating Load

Voltage fluctuation and power quantities fluctuations are major power quality disturbances caused by fluctuating load. They are used to reveal loading condition, respectively, as follows.

### 4.1 Voltage fluctuation

In a short duration, a voltage fluctuation waveform can be described as

$$v(t) = \sqrt{2}V_{rms} [1 + \frac{1}{2} \sum_n \Delta V_{fn} \sin(2\pi f_n t + \varphi_n)] \sin(2\pi f_{sys} t) \quad (6)$$

where  $f_{sys}$  is the fundamental frequency (power frequency),  $V_{rms}$  is the RMS value, and  $\Delta V_{fn}$  is fluctuation component of the amplitude modulation frequency  $f_n$ . For the voltage fluctuation limitation, we only need to consider  $f_n$  in the range of 0.1Hz~30Hz.

The definitions of voltage deviation  $\Delta V$  is

$$\Delta V = \sqrt{\sum_n (\Delta V_{fn})^2} \quad (7)$$

## 4.2 Power Quantities [21]

It is required to preserve several values of power quantities after data compression to represent the characteristics of fluctuating load. For a three-phase three-wire load under non-sinusoidal and unbalanced conditions, the arithmetic apparent power is

$$S_A = S_R + S_S + S_T = V_R I_R + V_S I_S + V_T I_T \quad (8)$$

If only fundamental components are considered, the fundamental active power and reactive power are, respectively, as follows.

$$P_1 = P_{R1} + P_{S1} + P_{T1} \quad (9)$$

$$Q_1 = Q_{R1} + Q_{S1} + Q_{T1} \quad (10)$$

Therefore, the corresponding fundamental apparent power is given by

$$S_1 = \sqrt{P_1^2 + Q_1^2} \quad (11)$$

To reveal harmonic condition, the non-fundamental arithmetic apparent power can be defined as

$$S_{AN} = \sqrt{S_A^2 - S_1^2} \quad (12)$$

Additionally, the effective representation of three-phase fundamental voltages and currents can be given by

$$V_{e1} = \sqrt{\frac{V_{R1}^2 + V_{S1}^2 + V_{T1}^2}{3}} \quad (13)$$

$$I_{e1} = \sqrt{\frac{I_{R1}^2 + I_{S1}^2 + I_{T1}^2}{3}} \quad (14)$$

Then the fundamental effective apparent power is defined as

$$S_{e1} = 3V_{e1}I_{e1} \quad (15)$$

It is noted that  $S_{e1}$  is different with  $S_1$ . When there is an unbalanced situation, the fundamental positive-sequence apparent power is defined as

$$S_1^+ = 3V_1^+ I_1^+ \quad (16)$$

Where  $V_1^+$  and  $I_1^+$  are the fundamental positive-sequence components. Therefore the unbalanced condition can be represented by the fundamental unbalanced apparent power as follows.

$$S_{1U} = \sqrt{S_{e1}^2 - S_1^{+2}} \quad (17)$$

## 5 Test of Voltage Fluctuation Waveforms

In order to reveal the efficiency of data compression, the compression ratio (CR) is defined as

$$CR = \frac{\text{original file size}}{\text{compressed file size}} \quad (18)$$

The evaluation of the signal quality after reconstruction can be achieved by the normalized mean-square error (NMSE). A lower NMSE means a smaller error between the reconstruction signal and the original one. It is given by

$$NMSE = \frac{\|C_o[n] - \hat{C}_o[n]\|^2}{\|C_o[n]\|^2} \quad (19)$$

Before the DWT approach with NEZW coding, threshold (TH) coding [22], and vector quantization (VQ) coding [22] are applied to practical waveforms of fluctuating load, the abilities of preserving voltage fluctuation information are examined by some given waveforms. The description about TH coding and VQ coding is given in Appendix. TABLE I shows the compression results of NEZW coding, TH coding, and VQ coding that are applied to a given voltage fluctuation waveform. The threshold factor  $u=0.5$  is applied to the TH coding. The codebook sizes of VQ are given in Appendix. The denotation  $MRA_x\text{-NEZW}2^{-y}$  implies the  $x$ -level MRA with NEZW coding and its threshold value down to  $1/(2^y)$ . Similarly,  $MRA_x\text{-TH}$  and  $MRA_x\text{-VQ}$  mean the  $x$ -level MRA with TH coding and VQ coding, respectively. Since there are so many kinds of wavelet basic functions, Biorthogonal-3.3 is chosen through an evaluation for the following study.

The voltage amplitude modulation components are listed in the second row of TABLE I. Some observations can be obtained.

- (1) With a given threshold in the NEZW, the CR values and the errors increase with increasing decomposition levels.
- (2) With a fixed decomposition level, the CR values and the errors decrease with decreasing threshold.
- (3) With a same resolution level (MRA3), the NEZW coding is the best and the VQ coding is the worst in data compression to effectively keep accuracy of voltage fluctuation values.

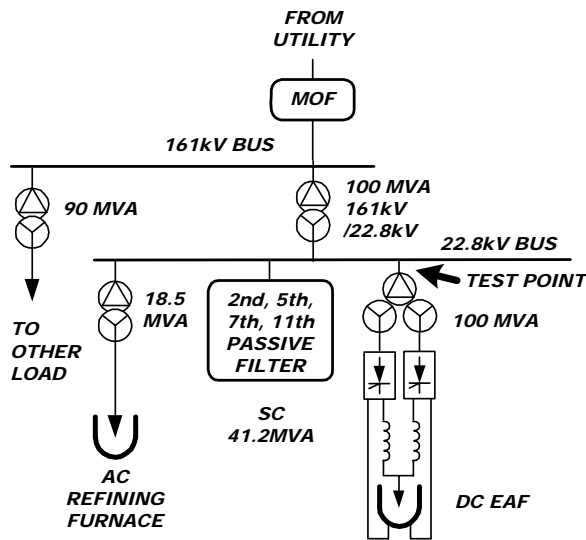


Fig. 4. One-line diagram of the DC electric arc furnace steel plant.

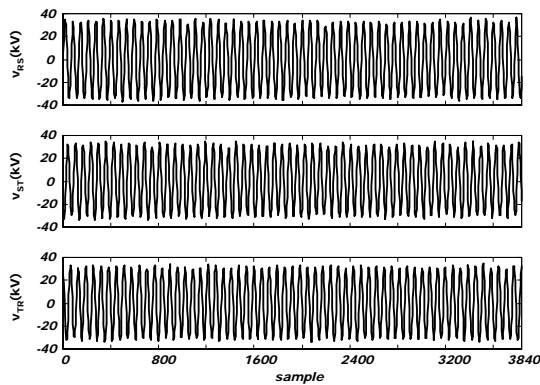


Fig. 5. 60-cycle voltage waveforms measured at DC EAF feed line.

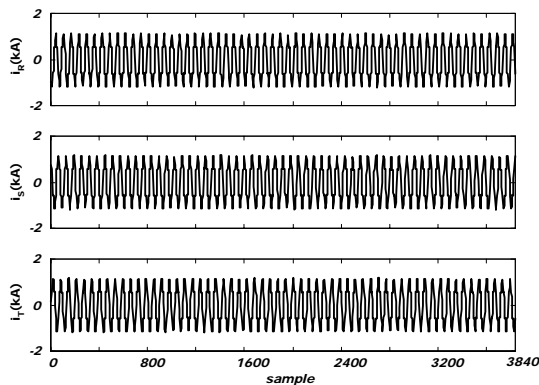


Fig. 6. 60-cycle current waveforms measured at DC EAF feed line.

## 6 Compression of DC Furnace Field Measurement Waveforms

The data compression approaches are applied to field measured voltage and current waveforms of a steel-making plant with a DC EAF. Figure 4 shows the one-line diagram of the plant. Only for illustration, the

60-cycle three-phase voltage and current waveforms (64 samples per cycle, total 3840 samples) measured at the EAF feeder during the melting-down period are shown in Fig. 5 and Fig. 6, respectively. They reveal that the fluctuations of voltage and current waveforms are obvious. In total, 3,456,000 samples were recorded in the 15-minute measurement and used to reveal the performance of data compression. Considering a lower NMSE and an acceptable CR, MRA3\_NEZW2<sup>-4</sup>, MRA3\_TH, and MRA3\_VQ are chosen for comparison.

### 6.1 Voltage fluctuation values

The data compression results of three-phase voltage and current waveforms are listed in TABLE II. For the voltage fluctuation waveform, the MRA3\_NEZW2<sup>-4</sup> coding has the best performance, then the MRA3\_TH. Figure 7 shows the  $\Delta V$  values of the original voltage waveform and errors of reconstructed waveforms in the 15-minute period.

### 6.2 Power quantities

Each first figure within Figs.8-10 gives the deviations of  $S_A$ ,  $S_{AN}$ , and  $S_{IU}$  in the 15-minute measurement period, respectively. They are calculated by the original recorded data of voltage and current waveforms. The second column of TABLE III shows the integral true values of  $P_1$ ,  $Q_1$ ,  $S_1$ ,  $S_A$ ,  $S_{AN}$ , and  $S_{IU}$  of the 15-minute measurement data, respectively. The other figures within Figs. 8-10 give deviations of absolute errors of those powers between the original and reconstructed waveforms of the 15-minute measurement data. The third, the fourth, and the fifth column of TABLE III also give the integral absolute errors and percentage errors of those power quantities between the original and reconstructed waveforms of the 15-minute measurement data. It can be found that the MRA3\_NEZW2<sup>-4</sup> coding and MRA3\_TH coding have lower errors than MRA3\_VQ one. Especially, the MRA3\_NEZW2<sup>-4</sup> coding almost reflects the fundamental power quantities truly, and the integral errors are even lower than 0.1%. While the integral error of  $S_{AN}$  is a little higher, that of  $S_{IU}$  is not. However, the MRA3\_VQ coding would cause larger errors, where the integral error of  $S_{IU}$  is even up to 356%.

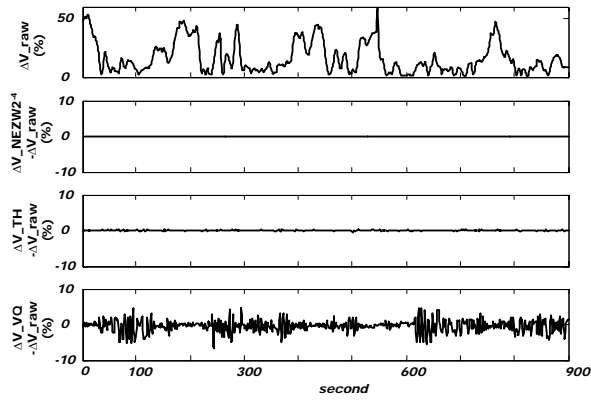


Fig. 7. The  $\Delta V$  values of the original measured voltage waveform and their errors versus to reconstructed waveforms of three coding methods in the 15-minute period of DC EAF feed line.

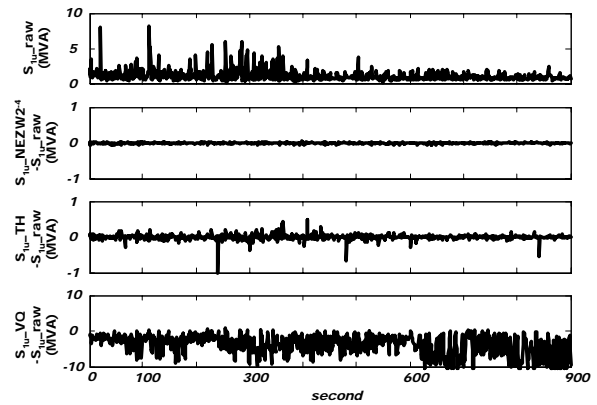


Fig. 10. The  $S_{lu}$  values of the original measured current waveform and their errors versus to reconstructed waveforms of three coding methods in the 15-minute period of DC EAF feed line.

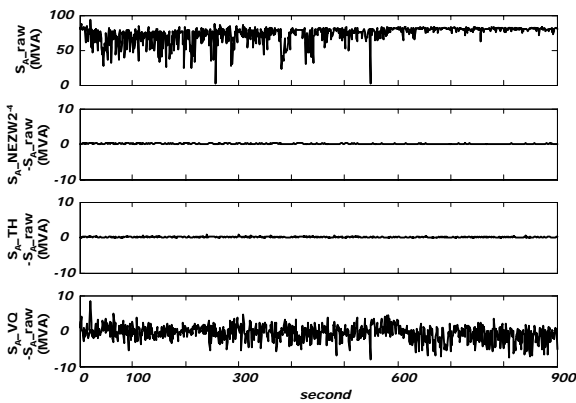


Fig. 8. The  $S_A$  values of the original measured current waveform and their errors versus to reconstructed waveforms of three coding methods in the 15-minute period of DC EAF feed line.

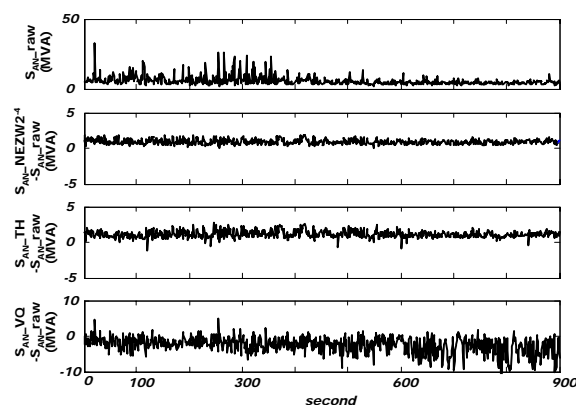


Fig. 9. The  $S_{AN}$  values of the original measured current waveform and their errors versus to reconstructed waveforms of three coding methods in the 15-minute period of DC EAF feed line.

## 7 Compression of Railroad Tracking Load Field Measurement Waveforms

The data compression approaches are also applied to field measured voltage and current waveforms of a substation in the Taiwan Railway electrification system. Figure 11 shows the one-line diagram of Shulin substation in the Taiwan Railway electrification system. This substation employs two identical Le Blanc transformers in parallel operation, which transform the 69kV three-phase powers to 27.5kV two-phase powers for electric tracking loads. The capacity of each transformer is 15MVA. Two independent incoming 69kV feeds (named Red and White feed lines, respectively) are used from a 69kV high voltage grid of the Taiwan Power Company (Taipower). Only for illustration, the 60-cycle three-phase voltage and current waveforms (64 samples per cycle, total 3840 samples) measured at the Red feed line are shown in Fig. 12 and Fig. 13, respectively. Due to the Le Blanc transformers supply two single-phase tracking loads, the unbalanced three-phase current waveforms are obvious. In total, 3,456,000 samples were recorded in the 15-minute measurement and used to reveal the performance of data compression. Considering a lower NMSE and an acceptable CR, MRA3\_NEZW<sup>-4</sup>, MRA3\_TH, and MRA3\_VQ are chosen for comparison.

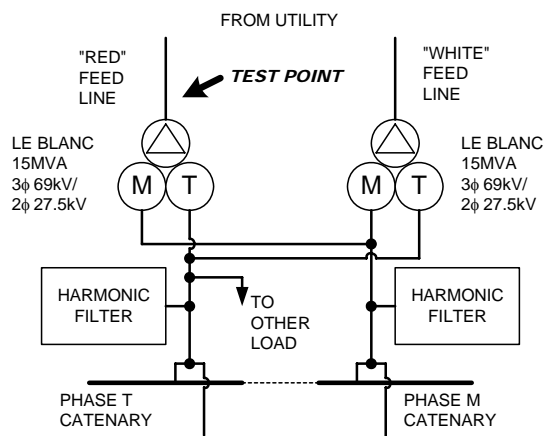


Fig. 11. One-line diagram of Shulin substation in Taiwan Railway electrification system.

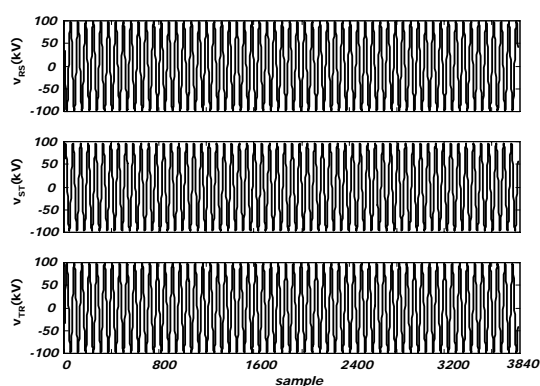


Fig. 12. 60-cycle voltage waveforms measured at Shulin substation feed line.

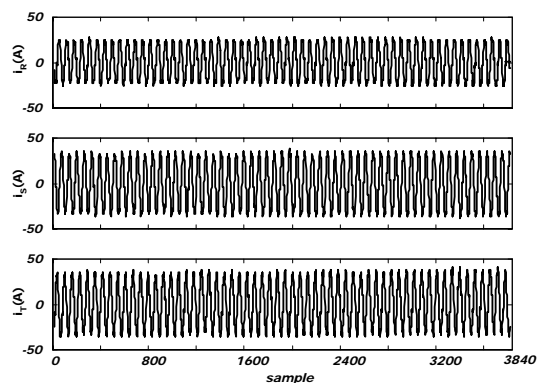


Fig. 13. 60-cycle current waveforms measured at Shulin substation feed lin

### (a) Voltage fluctuation values

The data compression results of three-phase voltage and current waveforms are listed in TABLE IV. Whatever the voltage fluctuation waveform, the results are similar to those as mentioned above DC EAF. That

is, the MRA3\_NEZW<sup>2-4</sup> coding is suitable for both voltage fluctuation waveforms in data compression. While, the MRA3\_TH coding is only suitable for voltage fluctuation waveform, the MRA3\_VQ coding is only good for current waveform.

### (b) Power quantities

The second column of TABLE V shows the integral true values of  $P_1$ ,  $Q_1$ ,  $S_1$ ,  $S_A$ ,  $S_{AN}$ , and  $S_{IU}$  of the 15-minute measurement data, respectively. The third, the fourth, and the fifth column of TABLE V also give the integral absolute errors and percentage errors of those power quantities between the original and reconstructed waveforms of the 15-minute measurement data. It can be found that the MRA3\_NEZW<sup>2-4</sup> coding and MRA3\_TH coding have lower errors than MRA3\_VQ one. Especially, the MRA3\_NEZW<sup>2-4</sup> coding almost reflects the fundamental power quantities truly, and the integral errors are even lower than 0.01%. While the integral error of  $S_{AN}$  is a little higher, that of  $S_{IU}$  is not. However, the MRA3\_VQ coding would cause larger errors, where the integral error of  $S_{IU}$  is even up to 17%.

## 8 Conclusion

Since the voltage and current waveforms of fluctuating load may be different cycle by cycle, the compression ratios of traditional data compression methods may be not large to keep enough data information. The data compression method using the normalized embedded zero-tree wavelet (NEZW) coding has been presented to be effective in reducing the data size in recording waveforms of a DC EAF and a railroad tracking load. This approach is better than conventional methods. It gives excellent ability to preserve information of voltage fluctuation and power quantities. From the computation results of the field measurement voltage and current waveforms, this method can reduce data memory size near to 15% while almost keep power quality characteristics. It is very suitable to be applied to power quality instruments in long duration load monitoring.

### References:

- [1] Y. Wang and J. Jiang, Mitigation of Electric Arc Furnace Voltage Flicker using Static Synchronous Compensator, *WSEAS Trans. on Power Systems*, Vol. 1, Issue 10, 2006, pp. 1734-1739.
- [2] R. Faranda, M. Giussani, and G. Testin, RC Filters Employment for the Protection of Industrial Arc Furnace Transformers during Switching-off Operations, *WSEAS Trans. on*

- Heat and Mass Transfer*, Vol. 1, Issue 8, 2006, pp. 699-706.
- [3] S.A. Sufliis, I.E. Chatzakis, F.V. Topalis, and M.B. Kostic, Scenarios for a Large Scale Installation of Compact Fluorescent Lamps: Influence on the Power Quality, *WSEAS Trans. on Circuits and Systems*, Vol.3, Issue 5, 2004, pp. 1386-1391.
- [4] W.Z. Li, W. Liao, and P. Han, Application of Wavelet Network for Detection and Localization of Power Quality Disturbances, *WSEAS Trans. on Power Systems*, Vol. 1, Issue 12, 2006, pp. 2029-2034.
- [5] G. T. Heydt, *Electric power quality*, Stars in a Circle Publications, 2nd edition, Indiana, USA, 1994.
- [6] *IEEE recommended practices and requirements for harmonic control in electrical power system*, IEEE Standard 519-1992, New Jersey, USA, 1993.
- [7] *Limitation of voltage fluctuations and flicker in low-voltage power supply systems for equipment with rated current greater than 16A*, IEC 61000-3-5, Electromagnetic compatibility (EMC), part 3: Limits-Section 5, 1994.
- [8] S. R. Huang and B. N. Chen, Harmonic Study of Le Blanc Transformer for Taiwan Railway Electrification System, *IEEE Trans. on Power Delivery*, vol. 14, no. 3, 1999, pp.767-772.
- [9] K. Sayood, *Introduction to data compression*, 2<sup>nd</sup> ed., San Francisco: Morgan Kaufmann, 2000.
- [10] T. B. Littler and D. J. Morrow, Wavelets for the analysis compression of power system disturbances, *IEEE Trans. on Power Delivery*, vol. 14, no. 2, 1999, pp. 358-364.
- [11] S. Santoso, E. J. Powers, and W. M. Grady, Power quality disturbance data compression using wavelet transform methods, *IEEE Trans. on Power Delivery*, vol. 12, no.3, 1997, pp.1250-1257.
- [12] S. Santoso, W. M. Grady, E. J. Powers, J. Lamoree, and S. C. Bhatt, Characterization of distribution power quality events with Fourier and wavelet transforms, *IEEE Trans. on Power Delivery*, vol. 15, no. 1, 2000, pp. 247-254.
- [13] A. M. Gaouda, M. M. A. Salama, M. R. Sultan, and A. Y. Chikhani, Power quality detection and classification using wavelet-multiresolution signal decomposition, *IEEE Trans. on Power Delivery*, vol. 14, no. 4, 1999, pp. 1469-1476.
- [14] C. Christopoulos, A. N. Skodras, and T. Ebrahimi, "the JPEG2000 still image coding system: an overview," *IEEE Trans. on Consumer Electronics*, vol. 46, no. 4, 2000, pp. 1103-1127.
- [15] Bryan E. Usevitch, A tutorial on modern lossy wavelet image compression: foundations of JPEG2000, *IEEE Signal Processing Magazine*, Sept. 2001, pp.22-35.
- [16] J. M. Shapiro, Embedded image coding using zerotrees of wavelet coefficients, *IEEE Trans. Signal Processing*, vol. 41, no. 12, 1993, pp.3445-3462.
- [17] D. Zhao, Y. K. Chan, and W. Gao, Low-complexity and low-memory entropy coder for image compression, *IEEE Trans. on Circuits and Systems for Video Technology*, vol. 11, no. 10, 2001, pp. 1140-1145.
- [18] X. Wang, G. Wu, and X. Lin, Wavelet image coding with lattice vector quantization, in *Proc. 1996, 3<sup>rd</sup> International Conference on Signal Processing*, vol. 2, pp. 966-969.
- [19] Y. Linde, A. Buzo, and R. Gray, An algorithm for vector quantizer design, *IEEE Trans. on Communications*, vol. 28, no. 1, 1980, pp. 84-95.
- [20] M. L. Hilton, Wavelet and Wavelet Packet Compression of Electrocardiograms, *IEEE Trans. on Biomedical Engineering*, Vol. 44, No. 5, 1997, pp.394-402.
- [21] *IEEE Std 1459-2000*, IEEE Trial-Use Standard Definitions for the Measurement of Electric Power Quantities Under Sinusoidal, Nonsinusoidal, Balanced, or Unbalanced Conditions, New York, 2000.
- [22] C. J. Wu and T. H. Fu, Data compression applied to electric power quality tracking of arc furnace load, *Journal of Marine Science and Technology*, Vol. 11, No. 1, March, 2003, pp. 39-47.

#### Appendix

##### A: Threshold (TH) coding

In the s-level MRA decomposition and reconstruction,  $C_{s-1}[n]$  is resolved into  $C_s[n]$  and  $D_s[n]$ , and the high frequency band coefficients  $D_s[n]$  will be processed through a threshold coding. If their absolute values are lower than the threshold value, they are discarded. Generally the threshold value  $\eta_s$  is defined as

$$\eta_s = u \times \max\{|D_s[n]|\} \quad (A1)$$

where  $u$  is the threshold factor, and  $0 \leq u \leq 1$ . The output sequence values are given by

$$\hat{D}_s[n] = \begin{cases} D_s[n] & |D_s[n]| \geq \eta_s \\ 0 & |D_s[n]| < \eta_s \end{cases} \quad (A2)$$

Using this simple threshold method, the decomposition data in  $D_s[n]$  with absolute values less than  $\eta_s$  are regarded as noises and filtered out. Therefore, the stored data for reconstruction are non-zero parts from  $D_s[n]$ , addresses of data, and  $C_s[n]$ .

**B. Vector Quantization (VQ) coding**

This method divides the original signal into pieces and treats them as  $n \times 1$  vectors. The typical samples for the piece signal  $X$  are named the codevectors  $Y_j$ , where  $j=1, 2, \dots, M$ . The set of codevectors contribute to a codebook. The codevector  $Y_k$  to represent  $X$  is chosen from the codebook, which makes  $d(X, Y_k) \leq d(X, Y_j)$  for  $j=1, 2, \dots, M$ , where  $d(X, Y_j)$  represents the error between  $X$  and  $Y_j$ . The most popular method for evaluating error is using the square of Euclidean distance of the two vectors. Therefore

$$d(X, Y_j) = \|X - Y_j\|^2 = \sum_{l=1}^n (x_l - y_{jl})^2 \quad (A3)$$

where  $X = (x_1, x_2, \dots, x_n)^t$  and  $Y_j = (y_{j1}, y_{j2}, \dots, y_{jn})^t$ . After choosing  $Y_k$ , the index  $k$  will be expressed using  $\log_2 M$  bits and sent out. At the decoding terminal, there exists the same codebook, which makes it

possible to find  $Y_k$  after receiving the index  $k$ , and use  $Y_k$  to represent  $X$ . In the MRA decomposition and reconstruction, the codebook in each resolution level would be different. The most popular codebook design method is to use the Linde-Buzo-Gray (LBG) training. The lower frequency band coefficients may contain more energy, and they are more important to reconstruct the signal. As a result, the size of codebook for the lower frequency band coefficients should be larger. The codebook sizes of VQ coding in different MRA levels are given in TABLE A1.

TABLE A1 CODEBOOK SIZES

Level	$D_s$	$C_s$
s=1	2	64
s=2	4	32
s=3	8	16
s=4	4	8
s=5	2	8

TABLE I COMPRESSION RESULTS OF THE GIVEN VOLTAGE FLUCTUATION WAVEFORM

	$V_{rms}$	Amplitude Modulation Component					$\Delta V$ (%)	CR	NMSE
		$\Delta V_{01}$	$\Delta V_{05}$	$\Delta V_{10}$	$\Delta V_{15}$	$\Delta V_{30}$			
Given Value	1	0.031	0.052	0.08	0.047	0.003	11.08	/	/
MRA3_NEZW2 <sup>-5</sup>	1	0.031	0.052	0.08	0.047	0.003	11.08	6.92	5.57E-06
MRA3_NEZW2 <sup>-4</sup>	1	0.031	0.052	0.08	0.047	0.003	11.08	7.89	1.37E-05
MRA3_NEZW2 <sup>-3</sup>	1	0.031	0.051	0.079	0.046	0.029	11.06	7.95	1.40E-05
MRA4_NEZW2 <sup>-5</sup>	1	0.031	0.052	0.08	0.047	0.003	11.07	10.69	2.99E-05
MRA4_NEZW2 <sup>-4</sup>	1	0.031	0.051	0.079	0.047	0.003	11.05	11.54	5.10E-05
MRA4_NEZW2 <sup>-3</sup>	1	0.031	0.051	0.079	0.046	0.029	10.99	12.80	1.91E-04
MRA2_TH	1	0.031	0.052	0.08	0.047	0.003	11.08	3.75	4.95E-05
MRA3_TH	1	0.031	0.052	0.08	0.047	0.003	11.08	6.87	7.12E-05
MRA4_TH	1	0.03	0.05	0.077	0.045	0.003	10.66	11.9	2.11E-03
MRA2_VQ	1	0.027	0.052	0.077	0.046	0.004	10.72	3.54	3.00E-04
MRA3_VQ	1	0.016	0.041	0.061	0.031	0.007	8.17	4.23	2.10E-03
MRA4_VQ	1	0.019	0.028	0.044	0.020	0.010	5.98	4.70	3.55E-03

TABLE II COMPRESSION RESULTS OF FIELD MEASUREMENT VOLTAGE FLUCTUATION AND CURRENT WAVEFORMS IN A DC EAF(USING MRA3 ANALYSIS)

			NEZW2-4	TH	VQ
voltage waveform	$v_R$	CR	7.29	5.67	4.27
		NMSE	5.00E-05	1.10E-04	1.48E-02
	$v_S$	CR	7.41	6.64	4.27
		NMSE	4.50E-05	1.05E-04	6.68E-03
	$v_T$	CR	7.35	6.57	4.27
		NMSE	4.10E-05	1.00E-04	2.42E-02
current waveform	$i_R$	CR	5.97	5.27	4.27
		NMSE	1.14E-02	2.09E-02	1.71E-02
	$i_S$	CR	5.82	5.02	4.27
		NMSE	3.63E-03	6.83E-03	1.59E-02
	$i_T$	CR	5.31	5.13	4.27
		NMSE	3.73E-03	7.92E-03	8.45E-02
Average of CR			6.53	5.71	4.27
Average of NMSE			3.14E-3	6.00E-03	2.72E-02

TABLE III COMPRESSION RESULTS OF INTEGRAL POWER QUANTITY OF THE 15-MINUTE MEASUREMENT DATA AND THREE DATA COMPRESSION CODINGS IN A DC EAF (USING MRA3 ANALYSIS)

Integral Power Quantity	True Value	NEZW2-4 Absolute Error (% Error)	TH Absolute Error (% Error)	VQ Absolute Error (% Error)
$\sum P_1 \Delta t$ (kWh)	449.175	0.029 (0.006)	0.631 (0.141)	60.215 (13.4)
$\sum Q_1 \Delta t$ (kvarh)	-707.415	0.326 (0.046)	0.662 (0.094)	84.851 (12.0)
$\sum S_1 \Delta t$ (kVAh)	841.201	0.304 (0.036)	0.898 (0.107)	103.245 (12.3)
$\sum S_A \Delta t$ (kVAh)	897.240	2.468 (0.275)	5.048 (0.563)	101.852 (11.4)
$\sum S_{AN} \Delta t$ (kVAh)	304.227	7.126 (2.342)	13.371 (4.395)	18.401 (6.05)
$\sum S_{Iu} \Delta t$ (kVAh)	389.895	0.661 (0.170)	0.799 (0.205)	69.071 (17.7)

TABLE IV COMPRESSION RESULTS OF FIELD MEASUREMENT VOLTAGE FLUCTUATION AND CURRENT WAVEFORMS IN A RAILWAY SUBSTATION (ALL ARE MRA3 ANALYSIS)

			NEZW2-4	TH	VQ
voltage waveform	$v_R$	CR	7.29	5.67	4.27
		NMSE	5.00E-05	1.10E-04	1.48E-02
	$v_S$	CR	7.41	6.64	4.27
		NMSE	4.50E-05	1.05E-04	6.68E-03
	$v_T$	CR	7.35	6.57	4.27
		NMSE	4.10E-05	1.00E-04	2.42E-02
current waveform	$i_R$	CR	5.97	5.27	4.27
		NMSE	1.14E-02	2.09E-02	1.71E-02
	$i_S$	CR	5.82	5.02	4.27
		NMSE	3.63E-03	6.83E-03	1.59E-02
	$i_T$	CR	5.31	5.13	4.27
		NMSE	3.73E-03	7.92E-03	8.45E-02
Average of CR			6.53	5.71	4.27
Average of NMSE			3.14E-3	6.00E-03	2.72E-02

TABLE V COMPRESSION RESULTS OF INTEGRAL POWER QUANTITY OF THE 15-MINUTE MEASUREMENT DATA AND THREE DATA COMPRESSION CODINGS IN A RAILWAY SUBSTATION (ALL ARE MRA3 ANALYSIS)

Integral Power Quantity	True Value	NEZW2-4 Absolute Error (% Error)	TH Absolute Error (% Error)	VQ Absolute Error (% Error)
$\sum P_1 \Delta t$ (kWh)	449.175	0.029 (0.006)	0.631 (0.141)	60.215 (13.406)
$\sum Q_1 \Delta t$ (kvarh)*	-707.415	0.326 (0.046)	0.662 (0.094)	84.851 (11.995)
$\sum S_1 \Delta t$ (kVAh)	841.201	0.304 (0.036)	0.898 (0.107)	103.245 (12.274)
$\sum S_A \Delta t$ (kVAh)	897.240	2.468 (0.275)	5.048 (0.563)	101.852 (11.352)
$\sum S_{AN} \Delta t$ (kVAh)	304.227	7.126 (2.342)	13.371 (4.395)	18.401 (6.049)
$\sum S_{lu} \Delta t$ (kVAh)	389.895	0.661 (0.170)	0.799 (0.205)	69.071 (17.715)

\*Negative values in  $\sum Q_1 \Delta t$  denote leading reactive power.